Research Article Open Access

Linli Fan and Li Liu*

Dynamics of asymmetric star polymers under coarse grain simulations

https://doi.org/10.1515/epoly-2019-0064
Received July 22, 2019; accepted August 22, 2019.

Abstract: The asymmetric star polymers are studied by coarse grain simulations. Each polymer chain is represented by number of consecutive soft blobs and additional uncrossability constraints are added to prevent chain crossings. In this work two types of asymmetric star polymers with different backbone lengths are structured. Their dynamical properties are discussed by comparisons with corresponding linear chains, the one covers chain length along with the asymmetric arm through the branch point to one of the symmetric arm, or the backbone chain between two symmetric arm ends, or the largest linear possesses the same molecular weight of the entire star. To reveal the influence of the asymmetric arm length on their relaxation decay times, the autocorrelation function of the vectors from each branching point to corresponding asymmetric arm end are calculated, results are compared with the symmetric star having the same backbone chain.

Keywords: asymmetric star, coarse grain, polymer melts, polymer dynamics, dynamical properties

1 Introduction

Different types of architecture make polymers behave with various physical properties, such as the branched polymers have higher density compared with linear polymers, for the branches often make the chains too difficult to get close enough for having the intermolecular forces work effectively. Polymer chain dynamical and rheological properties corresponding to the topology differences have been found in plenty of experimental (1-5) and theoretical investigations (6-9). Besides, there are also many simulation works to reveal and predict the properties of polymer systems in different scales (10-17).

Star polymers, with one branch point connecting to several linear arms are always of great interests. They can be creatively synthesized in laboratory or largely produced from industry (18,19). There are two main structures in terms of the arm length, symmetric star with all the arms having the equal length or asymmetric star at least contains one arm in different length to others. Having the simplest branch structure, both of the symmetric and asymmetric star polymers have been studied in many works extensively (9-12,20).

Coarse graining method has been implemented to study the simplest architecture of symmetric three-arm star polymer (21,22). In this work, another member from the simplest architectures of linear or symmetric star polymer is investigated, namely three-arm asymmetric stars in which two of the arms have the same length and the third arm is relatively shorter or longer. One might expect that asymmetric three-arm star can cross over the behaviors between a symmetric star and a linear polymer of the same arm length as the length of the third arm is varied. Therefore the dynamics of asymmetric three-arm stars varying with the arm length is mainly studied.

2 Model and methods

In this study, the TWENTANGLEMENT model has been used, briefly, each of the coarse-grained particle (blob) represents the center of mass of 20 consecutive monomers. Thus an entire 3-arm asymmetric star can be written as $\mathbf{B}(\mathbf{B}_m)(\mathbf{B}_n)_2$, where the first symbol **B** stands for the branching point, and the two terms $(\mathbf{B}_m)$ and $(\mathbf{B}_n)_2$, contribute to the description of one asymmetric

* **Corresponding author: Li Liu,** Department of Information Science and Engineering, Dalian Polytechnic University, Dalian, P. R. China, e-mail: liu.li@dlpu.edu.cn
Linli Fan, Department of Information Science and Engineering, Dalian Polytechnic University, Dalian, P. R. China

and two symmetric linear arms. Subscripts m and n denote the number of blobs contained on each arm. In general, the 3-arm asymmetric stars can be built in two kinds of shape, taking $\mathbf{B}(\mathbf{B}_7)(\mathbf{B}_3)_2$ and $\mathbf{B}(\mathbf{B}_3)(\mathbf{B}_7)_2$ as examples shown in Figure 1.

Because of the coarse-graining, the equation of motion of the position of the blobs can be described by the simple first order Langevin equation, which involves the conservative forces $\mathbf{F}^C$ derived from the potential of mean force Φ,

$$\mathrm{F}_i^c = -\nabla_i \Phi \tag{1}$$

as well as the blob fiction $\boldsymbol{\xi}$ and random forces $\mathbf{F}^R$ with the usual statistical properties,

$$d\mathrm{R}_i = -\frac{1}{\xi}\mathrm{F}_i^c dt + \mathrm{F}_i^R \tag{2}$$

The fluctuation-dissipation theorem demands the relation between $\boldsymbol{\xi}$ and $\mathbf{F}^R$ given in Eq. 3 as a condition for thermal equilibrium at the temperature of T = 450 K:

$$\left\langle \mathrm{F}_i^R(t)\mathrm{F}_j^R(0)\right\rangle = 6k_B T\xi\delta_{ij}\delta(t) \tag{3}$$

where k_B is the Boltzmann constant, and $\langle \mathbf{F}_i^R(t)\rangle = 0$.

The potential of mean force can be approximately presented as a sum of three independent parts, $\boldsymbol{\phi}^b$, $\boldsymbol{\phi}^\theta$, and $\boldsymbol{\phi}^{nb}$, with the usual meaning of bonded potential, angular potential and non-bonded or van der Waals potential separately. Using microscopic simulations (23,24), the distribution function between bonded and non-bonded blobs can be determined. Hence, the potential of mean force can be obtained by taking minus k_BT times the logarithm of measured distributions of blobs, i.e. $\boldsymbol{\Phi} = -k_BT\ln P(\mathbf{R}^n)$.

In mesoscopic simulations, since each blob represents a large group of monomers, the interaction between blobs will become so weak that bond crossings may occur. To prevent such unrealistic event, an additional uncrossibility algorithm, called Twentanglement is developed (23). In short, this algorithm modifies the chain dynamics by introducing entanglement constraints on the crossing site of two elastic bonds. Because of the elasticity, the distance $\mathbf{R}_{i,i+1}$ between two bonded consecutive blobs will be replaced by the path length $L_{i,i+1}$. Through the path entanglement positions $\mathbf{X}_p$ are defined, and thus the path from blob i to blob i+1 can be updated as

$$L_{i,i+1}\left(\mathrm{R}^n, \mathrm{X}^p\right) = \left|\mathrm{R}_i - \mathrm{X}_1\right| + \left|\mathrm{X}_1 - \mathrm{X}_2\right| + \cdots + \left|\mathrm{X}_p - \mathrm{R}_{i+1}\right| \tag{4}$$

with n the blob number and p the number of entanglements. Consequently, the expression of bonded attractive potential is now changed to be the function of path length. The entanglement positions are updated along with the moving of pair blobs and will be fixed at the points with the equilibrium of forces in the system. This is carried out by the minimization of total attractive potential energy for the given configuration $\mathbf{R}^n$ of the blobs,

$$\phi^{att}\left(\mathrm{R}^n\right) = \min_{\mathrm{X}^p}\sum i\phi^b\left(L_{i,i+1}\left(\mathrm{R}^n, \mathrm{X}^p\right)\right) \tag{5}$$

In our algorithm, when an entanglement from one arm slips over a branch point, it is either annihilated, or locates on one of the correct arm of the other two, or gets entangled with both of the other two arms. Usually in the last case, one of the two is chosen randomly to entangle with and the other entanglement is ignored. All simulations were performed in cubic boxes with periodic boundary conditions. The mass density of polyethylene melt was kept constant as $\boldsymbol{\rho}$ = 0.761 g/cm^3. All numerical results presented in this paper were obtained with $\boldsymbol{\xi}$ = 8.0 ps^{-1}.

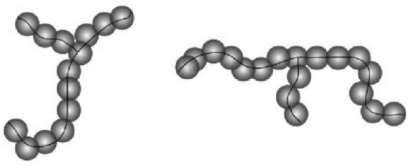

Figure 1: Schematic diagram of 3-arm asymmetric star: $\mathbf{B}(\mathbf{B}_7)(\mathbf{B}_3)_2$ two short arms and one long arm in 'Y' shape; or $\mathbf{B}(\mathbf{B}_3)(\mathbf{B}_7)_2$ one short arm and two long arms in 'T' shape.

3 Results and discussion

In this work the asymmetric star properties are presented from the comparisons with those linear polymers: one has the same length as the asymmetric linear arm; one backbone between two ends of symmetric arms; one is from the end of asymmetric arm to either end of the symmetric arm; and another long one possesses the same molecular weight of entire star. In Figure 2 the square of end-to-end distance

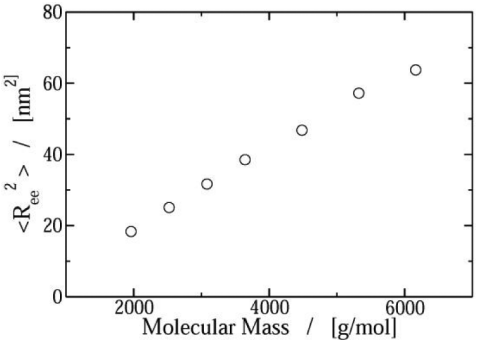

Figure 2: Linear chain end-to-end distance scaling property.

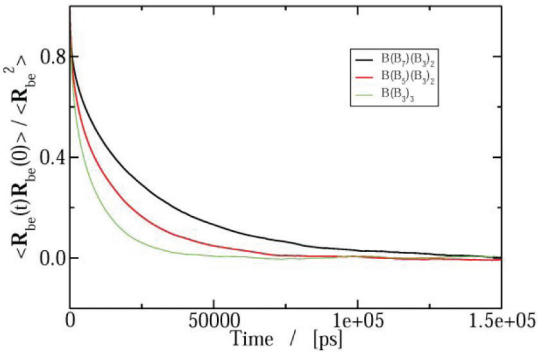

Figure 3: ACF for the unit vectors directed from the branch point to the end-points of the asymmetric arms of Y-shaped asymmetric stars.

of those linear chains are plotted, and the scaling property is to the power of ~1 along with the increasing of chain molecular mass.

Compared with those linear chains, the properties of asymmetric stars will be discussed mainly from the following aspects. Firstly, in order to understand the influence of the asymmetric arm on the star size and confirm the equilibrium of arm relaxation, the time dependent autocorrelation functions (ACF) for the unit vectors directed from each branch point to the end-point of the star asymmetric arms are calculated

$$R_{be}^2 = \left\langle \left(\mathrm{R}_b - \mathrm{R}_e \right)^2 \right\rangle \tag{6}$$

where $\mathbf{R}_b$ and $\mathbf{R}_e$ are the positions of branch point and asymmetric arm end for each configuration of the star polymer chain separately. Moreover, in melt system, the diffusive property is considered as an important physical quantity. It can be qualified by the diffusion coefficient extracted from the mean square displacement:

$$D(t) = \frac{1}{6t} \left\langle \left| \mathrm{R}_i^{cm}(t) - \mathrm{R}_i^{cm}(0) \right|^2 \right\rangle \tag{7}$$

where $\mathbf{R}_i^{cm}(t)$ is the center of mass position of chain i at time t, and the pointy brackets denote an average running through all the times and molecules.

3.1 Y-shaped asymmetric stars

The Y-shaped asymmetric stars have two short symmetric arms and one long asymmetric arm in the length of about two times larger than the short ones. By decreasing the number of blobs on the asymmetric arm, the three arms will have the equal length to form a symmetric star again.

In Figure 3 the autocorrelation function for the vector of asymmetric arms are presented. It is clear from this plot that the decay of the branch-end vectors for the asymmetric star arms becomes slower along with the increasing of arm length. At runtime about 1.5×10^5 ps, all these three curves drop to almost zero which assures that our system is well equilibrated. The similar timescale may be drawn as well as from the extracted diffusion coefficient curves from mean square displacements, shown in Figure 4.

Taking the contract with linear chains, the diffusive property of the center of mass of symmetric star $\mathbf{B}(\mathbf{B}_3)_3$ has been found very close to the linear $\mathbf{B}_{11}$, which contains the similar molecular weight, and slower than the backbone chain linear $\mathbf{B}_7$ (21), displayed in the top plot of Figure 4. While increasing the asymmetric arm length, the branch point gradually exhibits a topology constraint and starts to slow down the diffusion, shown in the middle and bottom plots in Figure 4. However, due to the limit length of the backbone chain $\mathbf{B}_7$, both of diffusion properties of the two asymmetric star $\mathbf{B}(\mathbf{B}_5)(\mathbf{B}_3)_2$ and $\mathbf{B}(\mathbf{B}_7)(\mathbf{B}_3)_2$ are more or less following the same trend as the symmetric star, i.e. diffuse similarly as the linear chain $\mathbf{B}_{13}$ which has the same molecular weight.

3.2 T-shaped asymmetric stars

The second type of asymmetric star studied in this work is in T shape, having two long symmetric linear $\mathbf{B}_7$ arms as the backbone and one short asymmetric arm $\mathbf{B}_3$ with half of the length of the symmetric arm. In this case, a relatively large symmetric star $\mathbf{B}(\mathbf{B}_7)_3$ will be recovered by increasing the length of the short arm.

For the three stars with the same length of backbone chain, it is clear to be seen from Figure 5 that the third arm moves slower when having the arm length increased, arm $\mathbf{B}_7$ in symmetric star $\mathbf{B}(\mathbf{B}_7)_3$ decays in a very slow way compared with arm $\mathbf{B}_3$ and $\mathbf{B}_5$ in asymmetric stars $\mathbf{B}(\mathbf{B}_3)(\mathbf{B}_7)_2$ and $\mathbf{B}(\mathbf{B}_5)(\mathbf{B}_7)_2$ respectively. The same trend can be seen from the appearance of scaled star diffusive motions in Figure 6.

From Figure 6, we can see that the diffusion coefficients for all the star polymers are the smallest on each figure from top to bottom. These stars move not only slower than their corresponding linear backbone chains but also after the linear chains with same molecular mass. This observation become clearer when we increase the asymmetric arm length from $\mathbf{B}_3$ to $\mathbf{B}_5$, and for the largest symmetric star $\mathbf{B}(\mathbf{B}_7)_3$ it moves the slowest beyond the time 10^5 ps.

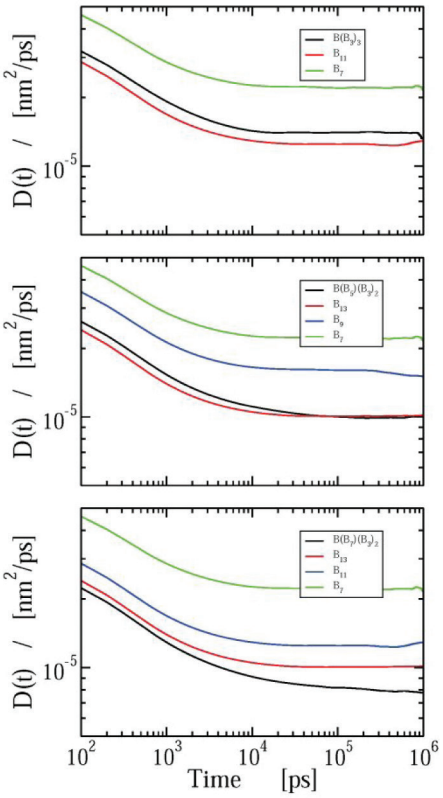

Figure 4: Time-dependent diffusion coefficients for symmetric star $\mathbf{B}(\mathbf{B}_3)_3$ and two asymmetric stars with various asymmetric arms, compared with the corresponding linear chains indicated in Figure 2.

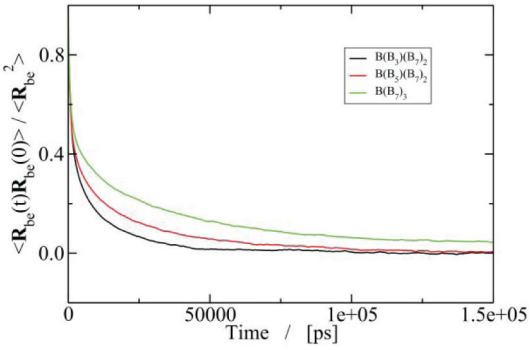

Figure 5: ACF for the unit vectors directed from the branch point to the end-points of the asymmetric arms of T-shaped asymmetric stars.

4 Conclusions

The dynamical trend of asymmetric stars has been studied by using coarse graining method. Results are presented by the comparisons with both linear and symmetric star topologies. It is found that for asymmetric stars with the same backbone chain, by increasing the asymmetric arm length, stars feel more and more branch point constraints that they behave a slower diffusion than corresponding

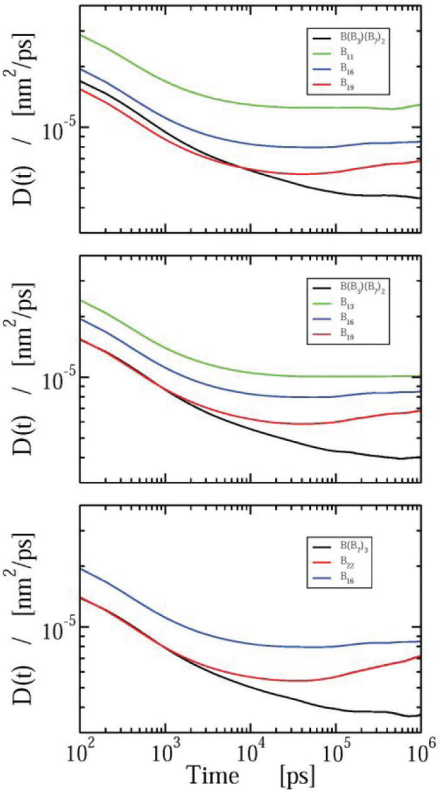

Figure 6: Time-dependent diffusion coefficients for symmetric star $\mathbf{B}(\mathbf{B}_7)_3$ and two asymmetric stars with various asymmetric arms, compared with the corresponding linear chains indicated in Figure 2.

linear chains, this trend is shown clearer to the asymmetric star with longer backbone chain.

In this work, it is clear to see that within our current simulation runtime, the relatively long linear or star polymers with arms in high molecular mass are not fully diffused or well relaxed. Extra simulation times are still needed for those polymers to get better statistics.

Acknowledgements: The authors acknowledge financial support from the National Natural Science Foundation of China (Grant: 21704010), the Natural Science Foundation of Liaoning Province (Grant: 2015010217-301), and the European Union's Seventh Frame-work Program (FP7) through the Marie Curie initial training network DYNamics of Architecturally Complex Polymers (Grant: 214627).

References

1. Pearson D.S., Ver Strate G., von Meerwall E., Schilling F.C., Viscosity and Self-Diffusion Coefficient of Linear Polyethylene. Macromolecules, 1987, 20, 1133-1141.
2. Pearson D.S., Fetters L.J., Graessley W.W., Ver Strate G., von Meerwall E., Viscosity and Self-Diffusion Coefficient of Hydrogenated Polybutadiene. Macromolecules, 1994, 27, 711-719.
3. Bartels C.R., Crist B., Fetters J., Graessley W.W., Self-diffusion in branched polymer melts. Macromolecules, 2002, 19(3), 4309-4311.
4. Pyckhout-Hintzen W., Allgaier J., Richter D., Recent developments in polymer dynamics investigations of architecturally complex systems. Eur. Polym. J., 2011, 47, 474-485.
5. Harmandaris V.A., Mavrantzas V.G., Theodorou D.N., Kröger M., Ramírez J., Öttinger H.C., et al., Crossover from the Rouse to the Entangled PolymerMelt Regime: Signals from Long, Detailed Atomistic Molecular Dynamics Simulations, Supported by Rheological Experiments. Macromolecules, 2003, 36, 1376-1387.
6. Rouse P.E., A Theory of the Linear Viscoelastic Properties of Dilute Solutions of Coiling Polymers. J. Chem. Phys., 1998, 108, 4628-4633.
7. De Gennes P.G., Scaling Concepts in Polymer Physics. Cornell University Press, New York, 1979.
8. Doi M., Edwards S.F., The Theory of Polymers Dynamics. Oxford Science Publications, U.K., 1986.
9. Frischknecht A.L., Milner S.T., Pryke A., Young R.N., Hawkins R., McLeish T.C.B., Rheology of Three-Arm Asymmetric Star Polymer Melts. Macromolecules, 2002, 35, 4801-4820.
10. Brown S., Szamel G., Computer simulation of three-arm star polymers. Macromol. Theor. Simul., 2000, 9, 14-19.
11. Masubuchi Y., Yaoita T., Matsumiya Y., Watanabe H., Primitive chain network simulations for asymmetric star polymers. J. Chem. Phys., 2011, 134, 775-S100.
12. Zhou Q. Larson R.G., Direct Molecular Dynamics Simulation of Branch Point Motion in Asymmetric Star Polymer Melts. Macromolecules, 2007, 40, 3443-3449.
13. Liu X., Zhou C., Xia H., Zhou Y., Jiang W., Dissipative particle dynamics simulation on the self-assembly of linear ABC triblock copolymers under rigid spherical confinements. e-Polymers, 2017, 17, 321-331.
14. Padding J.T., Briels W.J., Systematic coarse-graining of the dynamics of entangled polymer melts: the road from chemistry to rheology. J. Phys.-Condens. Mat., 2011, 23, 233101.
15. Hur K., Jeong C., Winkler R.G., Lacevic N., Hee R.H., Yoon D.Y., Chain Dynamics of Ring and Linear Polyethylene Melts from Molecular Dynamics Simulations. Macromolecules, 2011, 44(7), 2311-2315.
16. Jabbarzadeh A., Atkinson J.D., Tanner R.I., Effect of Molecular Shape on Rheological Properties in Molecular Dynamics Simulation of Star, H, Comb, and Linear Polymer Melts. Macromolecules, 2003, 36, 5020-5031.
17. Karayiannis N.C., Mavrantzas V.G., Hierarchical Modelling of the Dynamics of Polymers with a Nonlinear Molecular Architecture: Calculation of Branch Point Friction and Chain Reptation Time of H-Shaped Polyethylene Melts from Long Molecular Dynamics Simulations. Macromolecules, 2005, 38, 8583-8596.
18. Agostini S., Hutchings L., Synthesis and temperature gradient interaction chromatography of model asymmetric star polymers by the macromonomer approach. Eur. Polym. J., 2013, 49, 2769-2784.
19. Hsu J., Li C., Sugiyama K., Mezzenga R., Hirao A., Chen W., Synthesis and morphology of new asymmetric star polymers of poly[4-(9,9-dihexylfloren-2-yl)styrene]-block-poly(2-vinylpyridine) and their non-volatile memory device applications. Soft Matter, 2011, 7, 8440-8449.
20. Grest G.S., Fetters L.J., Huang J. Richter S.D., Star Polymers: Experiment Theory and Simulation". Adv. Chem. Phys.: Polymeric Systems, 1996, XCIV, 67-163.
21. Liu L., Padding J.T., den Otter W.K., Briels W.J., Coarse-grained simulations of moderately entangled star polyethylene melts. J. Chem. Phys., 2013, 138, 925.
22. Liu L., den Otter W.K., Briels W.J., Coarse-Grained Simulations of Three-Armed Star Polymer Melts and Comparison with Linear Chains. J. Phys. Chem. B, 2018, 122, 10210-10218.
23. Padding J.T., Briels W.J., Uncrossability constraints in mesoscopic polymer melt simulations: Non-Rouse behavior of $C_{120}H_{242}$. J. Chem. Phys., 2001, 115, 2846-2859.
24. Reith D., Pütz M., Müller-Plathe F., Deriving Effective Mesoscale Potentials from Atomistic Simulations. J. Comput. Chem., 2010, 24, 1624-1636.